Title

Development of a time-of-flight, decay and position-sensitive detector for FIONA

Journal

Nuclear Instruments and Methods in Physics Research Section A Accelerators Spectrometers Detectors and Associated Equipment, 1088

ISSN

0168-9002

Authors

Lykiardopoulou, EM
Orford, R
Campbell, CM
et al.

Publication Date

2026-08-01

DOI

10.1016/j.nima.2026.171478

Peer reviewed

Development of a time-of-flight, decay and position-sensitive detector for FIONA

E. M. Lykiardopoulou, R. Orford, C. M. Campbell, J. M. Gates, R. Krücken, E. Leistenschneider, J. L. Pore

Nuclear Science Division Lawrence Berkeley National Laboratory 1 Cyclotron Road Berkeley 94720 CA USA

Abstract

A decay and timing detector for superheavy elements has been developed at Lawrence Berkeley National Laboratory with the goal to become the main measurement detector of FIONA. It combines a double-sided silicon strip detector that provides decay energy and position information with a microchannel plate detector which determines the implantation time of the nuclei on the detector through the detection of secondary electrons emitted from the silicon detector upon impact. This new setup was simulated, constructed and tested offline, in a proof-of-principle setup using a beam of $^{216}Po^{+}$, the results of which are presented in this work. The new detector provides, for the first time in FIONA, sensitivity to isotopes beyond α emitters (and fissioning isotopes) and decay time information.

Keywords:

1. Introduction

The detection and study of SuperHeavy Elements (SHE, $Z \geq 104$) has been at the forefront of fundamental science for many decades. While the discovery of new elements still remains as one of the holy grails of the field, the measurements of a plethora of different quantities have been emerging to explain the vastly unknown properties of these exotic elements (for example see [1, 2, 3]).

At Lawrence Berkeley National Laboratory (LBNL), SHE are produced and detected at the 88-Inch Cyclotron facility. A beam of ions, such as Ca or Ti, is impinged on a rotating target made of a heavier element (typically

actinides), inducing fusion-evaporation reactions. The fusion-evaporation reaction products are separated from the unreacted beam and lighter transfer reaction products using the Berkeley Gas-filled Separator (BGS) [4] and are detected on a half-box detector assembly made of highly segmented Double-side Silicon-Strip Detectors (DSSD) named SuperHeavy RECoil detector (SHREC) [5]. While this setup is optimized for maximal transmission, and therefore very exotic element studies, as well as potential new element discoveries, it does not provide information on the properties of these elements other than the energy of their α decays, their branching ratios and their half-lives. In addition, this method of SHE detection cannot always unambiguously determine the identity of the produced element [6].

To this end, For the Identification Of Nuclide A (FIONA) spectrometer [7] was built to unambiguously determine the SHE produced by detecting their mass number, as well as to probe other important properties such as their chemical behavior [8]. To achieve that, the SHE have to be slowed down from energies of tens of MeV to thermal energies and then re-accelerated to a well-defined energy of a few keV. The first step of this process is achieved through collisions with a high purity He gas at a pressure of 150 Torr in the FIONA gas catcher. The slowed down ions are then bunched and further cooled in the subsequent Radio-Frequency Quadrupole (RFQ) trap filled with helium gas (approx. 1 mTorr). After approximately 50 ms, ions are ejected from the RFQ, re-accelerated and can be sent straight to the FIONA Decay Station for mass over charge (A/q) identification or can be bent 90 degrees towards the coupling beamline as can be seen in the schematic of Fig. 1.

Mass identification at the FIONA Decay Station is achieved by passing the ions through a trochoidal spectrometer, which consists of perpendicular electric and magnetic fields, providing a mass resolving power of approximately 250 [7]. Depending on their A/q, ions follow different trajectories through the spectrometer and exit at a slightly different angle. Based on this property, their A/q is determined by recording their position with respect to the position of a well-known calibrant, on a DSSD, at the exit of the trochoidal spectrometer.

However, due to their low energy of only a few keV, the ions cannot penetrate past the dead layer of the detector and therefore cannot induce a signal upon implantation. What is detected instead, are the α particles emitted from the decay of the ions that have been implanted in the dead layer. Typically, either the parent or the daughter α decay is observed. From these α particles, the decay energy and the position in the detector is derived with

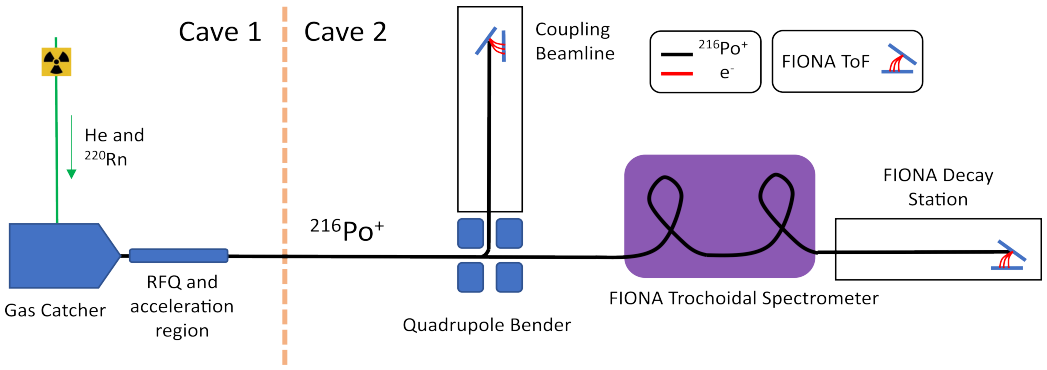

Figure 1: Schematic of the FIONA apparatus. ^{220}Rn is transported in the gas catcher with the He gas. In the gas catcher, ^{220}Rn decays into ^{216}Po. The ^{216}Po ions are confined due to a radio-frequency field and the He gas and later transported to the Coupling Beamline and the FIONA Decay Station.

the latter enabling the mass identification of the SHE species. While this technique has been proven successful through multiple experimental campaigns (for example [8, 9]), it limits FIONA from the determination of decay times; derived from the time difference between a decay and an implantation signal on the DSSD, and from sensitivity to non-α-decaying species.

Similar limitations have recently been overcome at the Radioactive Isotope Beam Factory (RIBF) facility of the Institute of Physical and Chemical Research (RIKEN) in Japan, through the development of the α-ToF detector [10]. This detector combines a commercial MagneToF detector with a silicon detector to provide both an implantation and a decay signal. More specifically, when SHE implant on the silicon detector, secondary electrons are emitted from the interaction of the superheavy ion and the material of the detector. The secondary electrons are then multiplied and guided towards an anode through the MagneToF detector, resulting in an implantation signal, while the SHE, which remains implanted in the silicon detector, eventually decays and if it is an α emitter, its α decay energy is recorded by the silicon detector.

Based on the principle of the RIKEN α-ToF detector, but with the additional capability of position resolution, necessary for FIONA mass identification measurements, a new detector has been constructed for FIONA, referred to as FIONA Time-of-Flight (ToF) detector. This article describes the design, commissioning and future plans for the FIONA ToF detector.

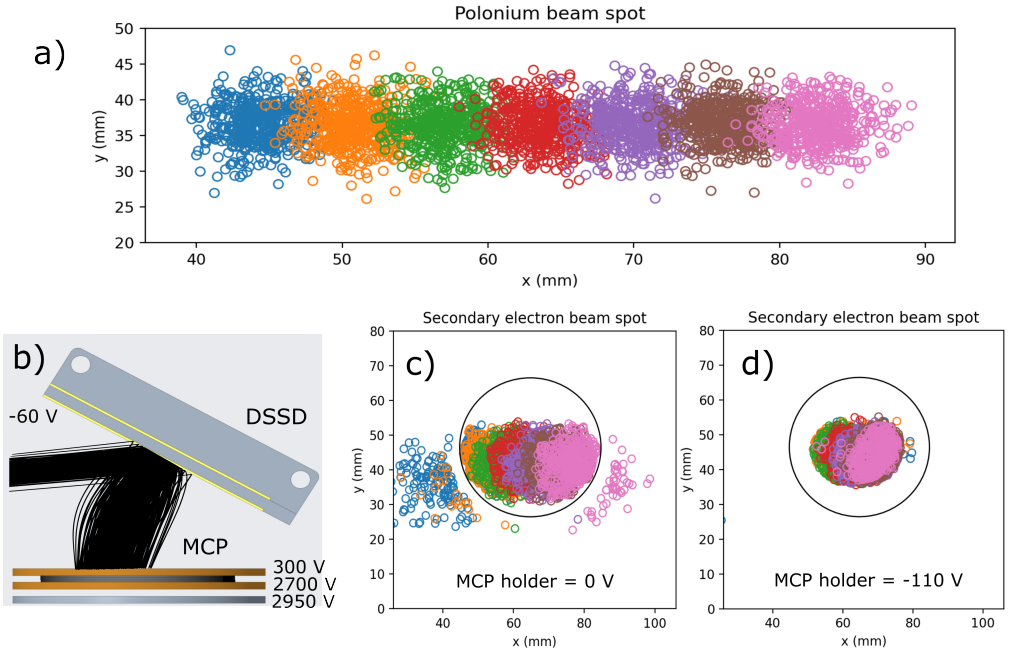

Figure 2: SIMION simulation results of electron transmission to the MCP. a) Simulated polonium beam spots on the DSSD. For each spot 500 $^{216}Po^{+}$ ions were simulated with a 3 keV energy. b) Ion trajectories to the DSSD and electron trajectories to the MCP. c) Electron spots on the MCP with the MCP holder at ground. d) Electron spots on the MCP with the holder voltage at -110V.

2. Concept and Design

The FIONA ToF detector allows for measuring both the α decay energy and position of ions passing through FIONA and adds the capability to determine when an ion impacts the detector. This has been achieved by combining two different detectors: a DSSD that provides the position and α decay information and a Micro-Channel Plate (MCP) detector that provides the Time-of-Flight (ToF) of the ions from the RFQ to the detector through the detection of secondary electrons that are emitted upon ion impact on the DSSD. The MCP signal from these secondary electrons acts as the implantation time signal on the detector and can be correlated with subsequent α decays on the DSSD to derive the decay time of the implanted species.

Simulations of the FIONA ToF detector were performed with SIMION2020 [11] to better understand the expected performance of the detector before

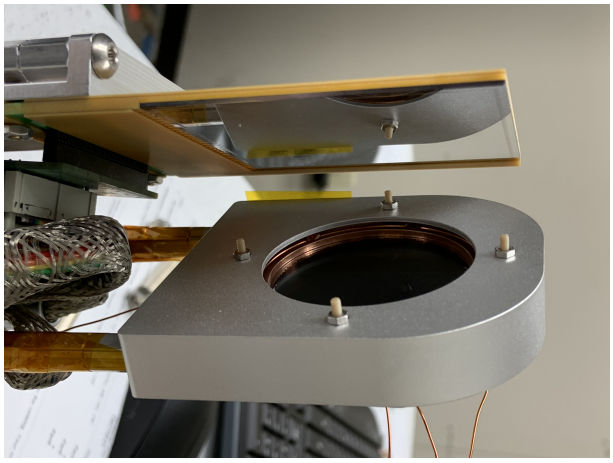

Figure 3: The FIONA ToF detector. The detector on the top is a 32 x 32 strip DSSD where ions are implanted and their decay is observed. The detector on the bottom, housed in an aluminum holder, is an MCP used for the detection of secondary electrons emitted during the implantation of ions in the DSSD. Both detectors are mounted on a 6-inch blank vacuum ConFlat flange using four threaded rods.

construction. The simulated geometry of FIONA ToF can be seen in Fig. 2 (b), where the two detectors were designed to be at a 30 degree angle allowing FIONA ToF to fit into a 6-inch ConFlat vacuum chamber while maximizing the spacial acceptance of the DSSD.

Recent experiments with FIONA have shown that the beam out of the acceleration region has a FWHM of 3.8(2) mm [12]. Based on this, simulations were performed where ions were ejected from an acceleration region with a 2 mm radius beamspot (1σ) and allowed to impact a DSSD. In the framework of this simulation, when an ion gets implanted on the DSSD a secondary electron with a $\approx$6 eV energy [13] is isotropically emitted. For the simulations, the MCP bias was chosen as recommended for electron detection and was set to 300 V for the front plate, 2700 V for the back plate and 2950V for the anode, while the DSSD was kept at -60 V. To better understand if the position that the ions impinge on the DSSD impacts the transmission to the MCP, the beam spots were simulated impacting the DSSD at various positions as can be seen in Fig. 2 (a). Figure 2 (b) shows the simulated ion trajectories to the DSSD and electron trajectories to the MCP, while Fig. 2 (c-d) show the position of the corresponding secondary electrons on the MCP for different focusing settings. The black circles represent the area of the MCP.

The focusing of the electrons from Fig. 2 (c) to Fig. 2 (d) is achieved by applying different bias voltages on the aluminum MCP housing frame shown in Fig. 3. In Fig. 2 (c) the secondary electron spots on the MCP are shown when the MCP frame is kept at ground, while in Fig. 2 (d) the MCP frame voltage is kept at -110 V. The two settings yield similar transmission efficiencies when the polonium ions implant on the DSSD at the middle strips of the DSSD. However, for ions being implanted closer to the edge of the DSSD, the transmission efficiency increases from 71% to 81 %, when biasing the frame to -110 V. While this simulation was specific to ^{216}Po, the electron transmission results are independent of the type of impinging ions and therefore it gives a general transmission efficiency for the FIONA ToF detector.

Using the results from the simulations as a guide, the FIONA ToF detector was constructed, and a picture of it is shown in Fig. 3. The DSSD was manufactured by Micron Semiconductor Ltd, with 32 front and 32 back strips, each having a 2 mm width. This detector covers an active area of 64 x 64 mm^2 and is used for the implantation of the SHE or other heavy ions and the observation of their subsequent α decays and/or fission. Specifically, the FIONA ToF DSSD provides the time, energy, and position of the α decays and fission events of the implanted species.

The MCP detector is a 40-mm diameter timing detector, developed by RoentDek (DET40) [14]. This detector includes two Hammamatsu MCP plates stacked in the Chevron configuration. The MCP is used as a ToF detector by detecting secondary electrons that are emitted when ions impinge on the DSSD. The MCP detector has a timing resolution of 100 ps [15], orders of magnitude smaller than the time spread of typical ion bunches from RFQ traps. The MCP detector itself is housed within an aluminum frame, seen in Fig. 3. Due to the simulations suggesting that biasing the holder can increase the transmission, the holder was wired to a feedthrough so that it can be kept either at ground or it can be biased.

Both detectors are mounted on a 6-inch ConFlat flange with four threaded aluminum rods. The signals from the DSSD are amplified using four mesytec MPR-16 lin-log pre-amplifiers, while the MCP signal, picked up from the front plate, is processed through a fast timing amplifier (FAMP1+) which amplifies the analog signals or through an amplifier and discriminator (LET1+) that generates NIM pulses of variable width. Both electronic modules are manufactured by RoentDek. The amplified signal traces are then digitized using two 64-channel CAEN VX2740 digitizers and recorded through the

CoMPASS software [16]. Both MCP and DSSD signals are recorded in a self-triggering mode with a recorded length of 30 μs. In addition, the RFQ ejection trigger is also digitized and recorded offering a start signal for the ToF measurement.

3. Characterization with lead and polonium ions and molecules

The FIONA ToF detector was tested using multiple configurations shown in Fig. 1 with $^{216}Po^{+}$ ions. These ions are generated as a decay product of a ^{232}U source that is located in the He-gas jet line. The ^{232}U undergoes a series of α decays to ^{220}Rn, which is then swept up in the He-gas jet and transported into the gas catcher that is kept at a pressure of $\approx$150 Torr. Inside the gas catcher, the ^{220}Rn decays into ^{216}Po, which is a short-lived ($T_{1/2}$ = 144.0(6) ms [17]), α-decaying isotope. The He gas and the Radio-Frequency (RF) field applied confine the ^{216}Po, some of which has a 1+ charge state. The $^{216}Po^{+}$ is then dragged towards an exit orifice of the gas catcher using a DC gradient field, where it is swept out of the gas catcher with the He gas. The He gas is differentially pumped away while the $^{216}Po^{+}$ is transported to the bunching RFQ through a transporting RFQ. In the bunching RFQ, $^{216}Po^{+}$ is cooled and bunched for up to 50 ms before being ejected and accelerated to an energy of approximately 3 keV.

After being ejected from the RFQ and accelerated, the ^{216}Po ions can be sent straight to the FIONA Trochoidal Spectrometer or can be bent 90° towards the Coupling Beam Line (CBL) using an electrostatic quadrupole bender. Figure 1 shows a schematic of the ions' path for these two detection locations. The FIONA ToF detector was initially installed and tested at the end of the CBL, then moved to the FIONA decay station. Results from the commissioning in both positions are described below.

3.1. Results from the Coupling Beamline

From the RFQ to the FIONA ToF at the CBL, the ions are guided and focused on the FIONA ToF DSSD with a series of steerers and lenses, and arrive at the detector approximately 70 μs after their extraction from the RFQ. When the ions arrive at the FIONA ToF DSSD, they are implanted approximately 5 nm beyond the surface, based on SRIM [18] calculations. Due to the fact that the dead-layer of the DSSD is approximately 1 μm, this implantation depth is not enough to induce an implantation signal pulse. However, the α decay of the implanted $^{216}Po^{+}$, and any of its associated

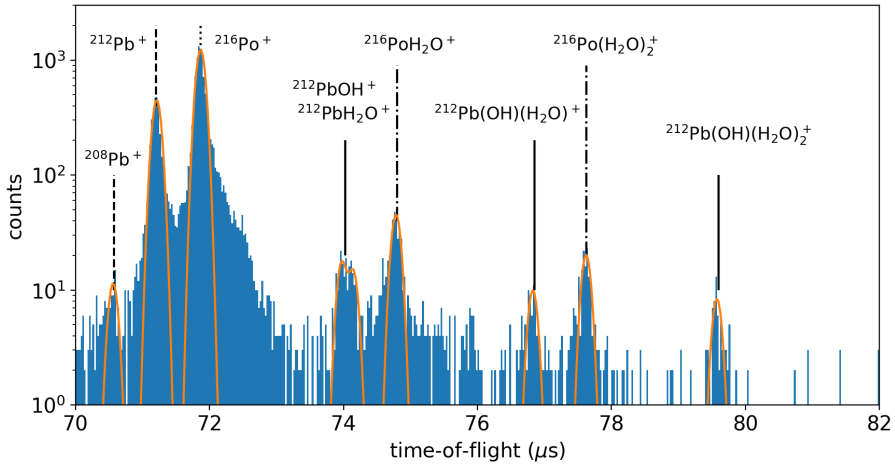

Figure 4: Time-of-Flight spectrum from secondary electrons using the FIONA ToF detector at CBL and the ^{220}Rn source.

molecular species, can be detected in the FIONA ToF DSSD, when those α-particles are emitted in the direction towards the DSSD, resulting in a 50% α detection efficiency.

The ToF of the beam, defined as the time difference between the signal induced by secondary electrons on the MCP and the RFQ trigger pulse is shown in Fig. 4. As all ions trapped in the RFQ start with approximately the same kinetic energy, the ToF of two species t_1 and t_2 of masses m_1 and m_2 at the FIONA ToF will be proportional to the square root of their mass ratio:

$$\frac{t_1}{t_2} = \sqrt{\frac{m_1}{m_2}} \tag{1}$$

From this formula, and knowing that the main species in the beam is ^{216}Po$^+$, the different peaks in the spectrum of Fig. 4 can be identified.

After calibrating the spectrum with ^{216}Po$^+$, the presence of its decay daughters ^{212}Pb$^+$ and ^{208}Pb$^+$ (dashed lines) as well as the molecules ^{216}PoH$_2$O$^+$ and ^{216}Po(H$_2$O)$_2$$^+$ can be verified. Based on previous FIONA mass identification measurements, these are molecules known to form in the system due to reactions with impurities in the He gas [8]. The rest of the peaks correspond to masses 229 u, 230 u, 247 u and 265 u and align with Pb(OH)$^+$,

$Pb(H_2O)^+$, $Pb(OH)(H_2O)^+$ and $Pb(OH)(H_2O)_2{}^+$, to which FIONA was previously insensitive to since ^{212}Pb decays by beta emission.

The ToF of the implanted ions can be correlated with the timing of α decays on the DSSD to determine the decay time of the α-decaying isotopes. Due to the fact that each detector has its own efficiency losses, the overall efficiency of the decay time measurement is going to be less than the detection efficiency of each individual detector. To estimate the total efficiency of FIONA ToF, for decay time measurements, we need to know i) the efficiency for detecting an α decay in the DSSD, ii) the combined secondary electron transmission efficiency from the DSSD to the MCP and the MCP detection efficiency, and iii) the expected losses due to correlation between the MCP and DSSD as the lifetime increases. The first is limited by the geometric efficiency as $\approx$50% of the α particles are emitted out of the face of the DSSD and therefore are not recorded. Second, SIMION simulations show that the transmission from the DSSD to the MCP reaches 100% depending on the position of the beam spot on the DSSD. Experimentally, we find that the maximum MCP detection efficiency in combination with the secondary electron transmission is not 100%, but rather 48(3)%, due to a maximum of 70% MCP detection efficiency, quoted by RoentDek, and 30% of other losses, possibly in the transmission of electrons to the MCP. Under ideal conditions, where (iii) is not a limiting factor, the efficiency of FIONA ToF for combined α-decays and ToF measurements is $\epsilon = 0.5 \cdot 0.48 = 0.24$ or 24%, where 0.5 is the geometric efficiency of the DSSD and 0.48 the efficiency of the MCP.

As the lifetime of the ion increases, one must also take into account the limit of correlation time between the MCP and the DSSD, which is mainly affected by the dark count rate of the MCP detector. MCP detectors usually have dark count rates of tens of Hz [15]. In addition, the noise rate can increase by placing them in noisy experimental environments. In FIONA, the MCP is in an environment with a number of high-voltage electronic switches and ionization vacuum gauges that increase the noise rate. To suppress it, a threshold is applied through the CoMPASS software. This threshold was scanned from 100 - 1000 least significant bit (lsb) [16] and we observed the rate at which we could detect secondary electrons originating from $^{216}Po^+$ and $^{212}Pb^+$ impacting FIONA ToF. As can be seen in Fig. 5, there is no loss in rate of ions impacting FIONA ToF as the threshold value is increased from 100 to 200. However, the rate of detection drops when the threshold value is increased to 300 and continues decreasing as the threshold value is raised. In our MCP, the total rate was measured to be 419.8(21) Hz at a threshold

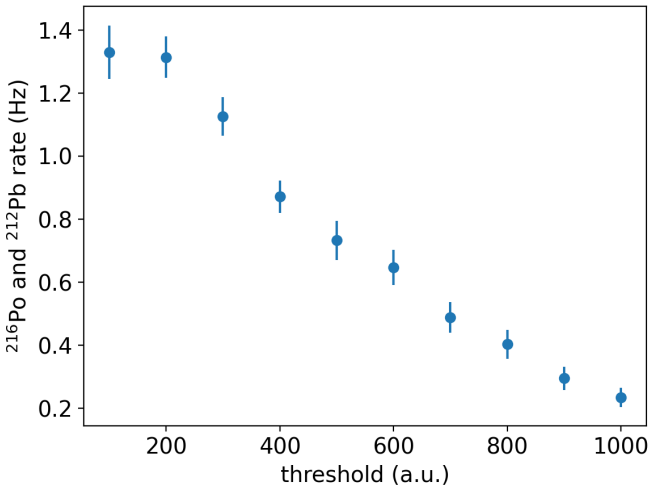

Figure 5: Rate of ^{216}Po and ^{212}Pb as a function of the software threshold value applied through CoMPASS [16].

value of 100, while when the threshold is 200, the total rate is 6.00(21) Hz, thus significantly reducing the noise rate that each real decay could correlate to.

Another way to reduce the correlations between real α decays on the DSSD and dark counts on the MCP is to only consider MCP events within a specific time window with reference to the RFQ extraction, when the beam is expected to arrive. For ^{216}Po, ^{212}Pb and their molecules, that is 65-85 μs after RFQ ejection. By looking at signals that arrive in this time window after ejection, our random coincidence rate drops from 0.3 dark counts per RFQ ejection to $1.2{\cdot}10^{-4}$.

With this rate of random coincidences, correlations can be performed between the MCP and the DSSD to derive the decay time of the implanted ions. This was done with ^{216}Po^{+} ions from the ^{220}Rn source, the results of which can be seen in Fig. 6. The left plot shows the correlation time between MCP signal (implant) and DSSD signal (α), as a function of the uncalibrated α energy. All the data points correspond to the decay of ^{216}Po, as it is the only α-decaying isotope in the beam. The plot on the right is a histogram of the correlation time for the same data. This histogram can be fitted to

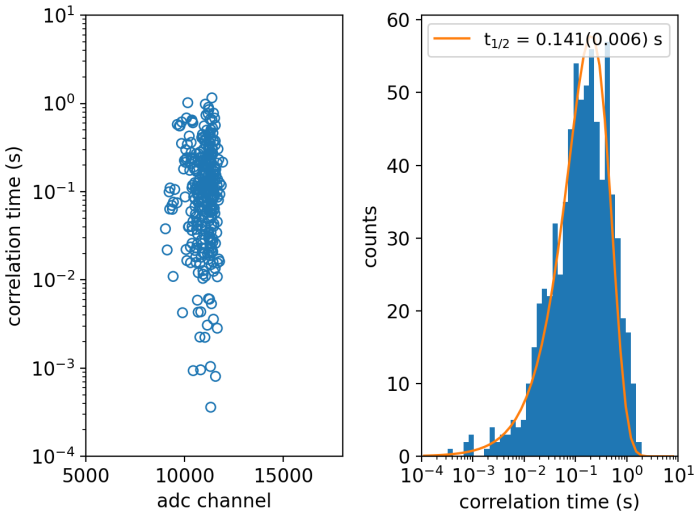

Figure 6: Correlation time versus uncalibrated energy scatter plot (left) and correlation time histogram (right) for the implanted polonium ions and their alpha decays, fitted with Equation 2 to derive the half-life of ^{216}Po.

extract the half-life of ^{216}Po using:

$$N = A\frac{tln2}{t_{1/2}}e^{-tln2/t_{1/2}} \tag{2}$$

where t is the correlation time and A and $t_{1/2}$ are fitting parameters with $t_{1/2}$ being the half-life. The result of fitting the data with Eq. 2 can be seen plotted in Fig. 6 with the orange line. The extracted half-life from the fit is $t_{1/2} = 0.141(6)$ s, well in agreement with literature ($t^{lit}_{1/2} = 0.1440(6)$ s [17]).

Finally, coincidences can be performed between α decays and ToF signals induced by secondary electrons emitted during α emission. The average coincidence time between α-decay signals and MCP signals for FIONA ToF was determined to be 2.4 μs with a FWHM of 0.4 μs. The average coincidence time includes offsets due to different cable lengths and signal processing differences between MCP and DSSD signals in CoMPASS and thus only provides an upper limit of the release and flight time of electrons to the MCP. In contrast, the FWHM reflects the real time spread of the secondary electrons as well as flight path differences of electrons released from different locations on the DSSD.

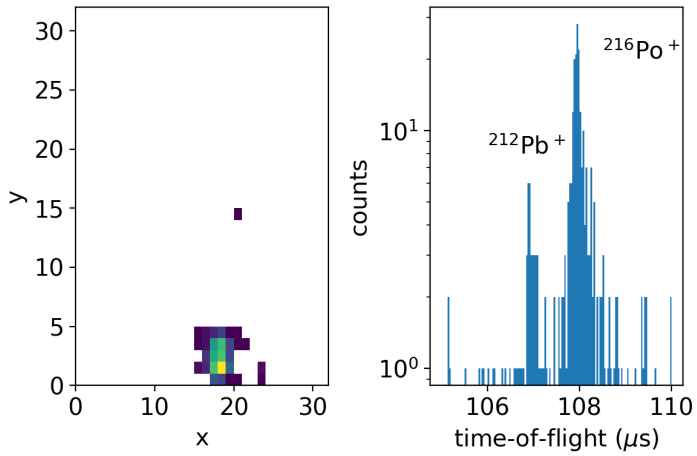

Figure 7: Position and ToF spectrum of the beam with FIONA ToF at the FIONA Decay Station. FIONA was set to transport mass 216 u, thus cutting down the water molecules shown in Fig. 4, while still allowing masses 216 u and 212 u to pass through.

3.2. Results from the FIONA Decay Station

As a second test,the FIONA ToF detector was placed after the trochoidal spectrometer, as pictured in Fig. 1. In this case, the acceptance through the spectrometer is limited to five mass units and individual masses are spacially separated in the horizontal direction by about 1 cm per mass unit as the troichoidal spectrometer has a resolving power of 250 [7]. Figure 7 shows the α-decay position and ToF spectrum from FIONA ToF for m = 216 u (^{216}Po) when placed at the FIONA decay station. While there is only one spot on the left, resulting from the α-decays of ^{216}Po, there are two ToF peaks on the ToF histogram (right) corresponding to the β-emitter ^{212}Pb and the α-emitter ^{216}Po.

4. Conclusions and Outlook

The FIONA ToF detector has been constructed and tested using an offline ^{232}U source providing ^{216}Po$^+$ ions to FIONA. It has enabled the detection of implantation events at the FIONA Coupling Beam Line and Decay Station which allows for the identification of beta-decaying and stable beam species and half-life measurements of α emitters and fissioning isotopes. A satisfactory efficiency of 48% for ToF measurements and 24% for decay time measurements has been achieved.

In the future, the FIONA ToF detector will be installed in a retractable configuration before the FIONA trochoidal spectrometer for broadband detection of the species that are extracted from the RFQ. This will enable a fast identification of the products of fusion-evaporation reactions in the BGS target and the molecules that then form during their storage in the RFQ. In addition, a second detector is under construction that will be placed at the FIONA Decay Station.

5. Acknowledgments

This work was supported by the Laboratory Directed Research and Development (LDRD) Program under the title: Development of an Advanced Superheavy Element Detector for FIONA. This work was supported in part by the U.S. Department of Energy, Office of Science, Office of Nuclear Physics under contract numbers DE-AC02-05CH11231. E.M.L. would like to thank Achim Czasch and Ottmar Jagutzki from RoentDek for their valuable support and feedback.

References

[1] E. Minaya Ramirez, et al., Direct mapping of nuclear shell effects in the heaviest elements., Science 337 (2012) 6099. doi:doi:10.1126/science.1225636.

[2] M. Block, M. Laatiaoui, S. Raeder, Recent progress in laser spectroscopy of the actinides, Progress in Particle and Nuclear Physics 116 (2021) 103834. doi:https://doi.org/10.1016/j.ppnp.2020.103834.
URL https://www.sciencedirect.com/science/article/pii/S0146641020300818

[3] R.-D. Herzberg, Spectroscopy of superheavy elements, Journal of Physics G: Nuclear and Particle Physics 30 (4) (2004) R123. doi:10.1088/0954-3899/30/4/R01.
URL https://doi.org/10.1088/0954-3899/30/4/R01

[4] K. Gregorich, Simulation of recoil trajectories in gas-filled magnetic separators, Nuclear Instruments and Methods in Physics Research Section A: Accelerators, Spectrometers, Detectors and Associated Equipment 711 (2013) 47–59. doi:https://doi.org/10.1016/j.nima.2013.01.020.
URL https://www.sciencedirect.com/science/article/pii/S0168900213000673

[5] P. Golubev, R. Orford, F. Garcia, D. Rudolph, L. Sarmiento, R. Clark, D. Cox, J. Gates, J. Gooding, M. Grebo, Y. Hrabar, T. Kramasz, M. McCarthy, M. Mohamed, J. Pore, Source characterization of a detector for heavy and superheavy nuclei, Nuclear Instruments and Methods in Physics Research Section A: Accelerators, Spectrometers, Detectors and Associated Equipment 1075 (2025) 170384. doi:https://doi.org/10.1016/j.nima.2025.170384.
URL https://www.sciencedirect.com/science/article/pii/S0168900225001858

[6] Gregorich, Kenneth, How good are superheavy element Z and A assignments?, EPJ Web Conf. 131 (2016) 06002. doi:10.1051/epjconf/201613106002.
URL https://doi.org/10.1051/epjconf/201613106002

[7] J. Gates, J. Pore, Studies of heavy and super heavy elements with FIONA: the broad impact of mass-number identifications., Eur. Phys. J. A 58 (2022) 196.
URL https://doi.org/10.1140/epja/s10050-022-00844-1

[8] J. Pore, J. Gates, D. Dixon, F. Garcia, J. Gibson, J. Gooding, M. McCarthy, R. Orford, Z. Shafi, D. Shuh, S. Sprouse, Direct identification of Ac and No molecules with an atom-at-a-time technique., Nature 644 (2025) 376–380. doi:https://doi.org/10.1038/s41586-025-09342-y.

[9] J. M. Gates, G. K. Pang, J. L. Pore, K. E. Gregorich, J. T. Kwarsick, G. Savard, N. E. Esker, M. Kireeff Covo, M. J. Mogannam, J. C. Batchelder, D. L. Bleuel, R. M. Clark, H. L. Crawford, P. Fallon, K. K. Hubbard, A. M. Hurst, I. T. Kolaja, A. O. Macchiavelli, C. Morse, R. Orford, L. Phair, M. A. Stoyer, First direct measurements of superheavy-element mass numbers, Phys. Rev. Lett. 121 (2018) 222501. doi:10.1103/PhysRevLett.121.222501.
URL https://link.aps.org/doi/10.1103/PhysRevLett.121.222501

[10] T. Niwase, M. Wada, P. Schury, H. Haba, S. Ishizawa, Y. Ito, D. Kaji, S. Kimura, H. Miyatake, K. Morimoto, K. Morita, M. Rosenbusch, H. Wollnik, T. Shanley, Y. Benari, Development of an "α-TOF" detector for correlated measurement of atomic masses and decay properties, Nuclear Instruments and Methods in Physics Research Section A: Accelerators, Spectrometers, Detectors and Associated Equipment 953

(2020) 163198. doi:https://doi.org/10.1016/j.nima.2019.163198.
URL https://www.sciencedirect.com/science/article/pii/S0168900219314901

[11] D. A. Dahl, simion for the personal computer in reflection, International Journal of Mass Spectrometry 200 (1) (2000) 3–25, volume 200: The state of the field as we move into a new millenium. doi:https://doi.org/10.1016/S1387-3806(00)00305-5.
URL https://www.sciencedirect.com/science/article/pii/S1387380600003055

[12] M. Grebo, et al., ^{51}V on ^{208}Pb, Under analysis.

[13] T. Kaneko, Secondary electron emission from metal surfaces by ion impact, Nuclear Instruments and Methods in Physics Research Section B: Beam Interactions with Materials and Atoms 67 (1) (1992) 655–658. doi:https://doi.org/10.1016/0168-583X(92)95893-V.
URL https://www.sciencedirect.com/science/article/pii/0168583X9295893V

[14] O. Jagutzki, V. Mergel, K. Ullmann-Pfleger, L. Spielberger, U. Spillmann, R. Dörner, H. Schmidt-Böcking, A broad-application microchannel-plate detector system for advanced particle or photon detection tasks: large area imaging, precise multi-hit timing information and high detection rate, Nuclear Instruments and Methods in Physics Research Section A: Accelerators, Spectrometers, Detectors and Associated Equipment 477 (1) (2002) 244–249, 5th Int. Conf. on Position-Sensitive Detectors. doi:https://doi.org/10.1016/S0168-9002(01)01839-3.
URL https://www.sciencedirect.com/science/article/pii/S0168900201018393

[15] RoentDek, Mcp detector with delay-line anode manual.
URL https://www.roentdek.com/manuals/

[16] See CAEN CoMPASS documentation at , https://www.caen.it/products/compass/.

[17] G. Audi, O. Bersillon, J. Blachot, A. Wapstra, The nubase evaluation of nuclear and decay properties, Nuclear Physics A 729 (1) (2003) 3–128, the 2003 NUBASE and Atomic Mass Evaluations. doi:https://doi.org/10.1016/j.nuclphysa.2003.11.001.
URL https://www.sciencedirect.com/science/article/pii/S0375947403018074

[18] J. F. Ziegler, Srim-2003, Nuclear Instruments and Methods in Physics Research Section B: Beam Interactions with Materials and Atoms 219-220 (2004) 1027–1036, proceedings of the Sixteenth International Conference on Ion Beam Analysis. doi:https://doi.org/10.1016/j.nimb.2004.01.208.
URL https://www.sciencedirect.com/science/article/pii/S0168583X04002587